Holocene fire regimes around the Altai-Sayan Mountains and adjacent plains: interaction with climate and vegetation types

Dongliang Zhang[1,2,3,*], Blyakharchuk Tatiana[4], Aizhi Sun[5,*], Xiaozhong Huang[6], Yuejing Li[1,2,3]

[1] *State Key Laboratory of Ecological Safety and Sustainable Development in Arid Lands, Xinjiang Institute of Ecology and Geography, Chinese Academy of Sciences, 818 Beijing South Road, Urumqi 830011, China.*

[2] *Research Center for Ecology and Environment of Central Asia, Chinese Academy of Sciences, 818 Beijing South Road, Urumqi 830011, China.*

[3] *University of Chinese Academy of Sciences, 19A Yuquan Road, Beijing 100049, China.*

[4] *Institute of Monitoring of Climatic and Ecological Systems, Siberian Branch of Russian Academy of Sciences, Tomsk, Russia.*

[5] *College of Earth and Planetary Sciences, University of Chinese Academy of Sciences, Beijing 100049, China.*

[6] *College of Earth and Environmental Sciences, Lanzhou University, Lanzhou, China.*

* Corresponding authors.

E-mail addresses: zhdl@ms.xjb.ac.cn (+86-18699198239) and aizhisun@ucas.ac.cn.

Abstract: The Altai-Sayan Mountains and adjacent plains (i.e., west Siberian Plain, Kazakhstan Hills and Junggar Basin) have experienced accelerated warming in recent decades, raising growing concerns about escalating wildfire risks. However, two key gaps hinder understanding: paleofire dynamics in western Mongolia are understudied and no comprehensive regional synthesis exists for charcoal influx across the Altai-Sayan ecoregion. To address these gaps, this study reconstructs the Holocene fire sequence in western Mongolia and systematically elucidates the spatiotemporal variations in charcoal influx across different vegetation zones of the Altai-Sayan Mountains and adjacent plains, as well as their coupling relationships with vegetation structure. The results reveal that Holocene declines in charcoal influx were driven by distinct mechanisms across subregions: above the forest limit in the central Altai Mountains, the decline was primarily controlled by temperature-mediated changes in woody biomass availability; in the western Sayan Mountains, it stemmed from the substantial expansion of fire-resistant *P. sylvestris*. Since ~2 cal. kyr BP, intensified anthropogenic disturbances (agricultural expansion and pastoral activities) have significantly increased fire frequency in the southeastern/western and northern Altai Mountains, the west Siberian Plain and the forest zones of the central Altai Mountains. Conversely, the marked decline in charcoal influx observed in the Khangai Mountains

may be closely associated with vegetation fragmentation caused by overgrazing. Our findings provide a long-term perspective on fire-vegetation-climate interactions, offering critical insights for sustainable land management in the Altai-Sayan Mountains and adjacent plains.

Key words: Charcoal influx; Fire activities; Vegetation; Altai-Sayan Mountains

1. Introduction

The North Europe-Siberia-Altai region is the core distribution area of boreal forest ecosystems, hosting over 90% of the continent's boreal forest biomass and terrestrial organic carbon stocks (Furyaev, 1996; Kasischke, 2000). Its dynamics are closely intertwined with the global climate system, forming a critical positive feedback loop. In 2021, wildfires in the global boreal forests released 1.76 $PgCO_2$, setting a historical record at that time (Zheng et al., 2023). Notably, the majority of carbon emissions from boreal forests originated from northern Eurasia. Carbon sequestration gain from a prolonged growing season may not offset the carbon loss caused by enhanced respiration and disturbances (Mo et al., 2023). This ecological transformation triggers critical climate feedback mechanisms through three primary pathways: carbon pool transformation, cascading infrastructure collapse and socioeconomic impacts resulting from fire-related mortality events (Ivanova et al., 2019; Jones et al., 2020). This shift not only threatens regional carbon balance but also significantly accelerates global warming by releasing massive amounts of greenhouse gases, underscoring the extreme urgency of protecting this ecosystem for stabilizing the global climate.

Boreal fire regimes are regulated by a tripartite control system, which specifically includes climatic drivers, ignition probability and fuel complex properties (Andela et al., 2017; Moritz et al., 2014). Although fires in this region currently remain predominantly moderate-intensity surface fires (Archibald et al., 2013), climate models predict that a shift in fire regimes is imminent. Fuel desiccation caused by climate warming, coupled with altered precipitation patterns, may drive the transition of fires to high-intensity crown fires through pyroconvective processes (Pitkanen et al., 2003). This transition will exert multidimensional impacts across different spatial scales, specifically manifested as follows: reduced albedo altering the surface energy balance, disrupting carbon-nutrient cycling dynamics, increasing aerosol emissions and fostering novel disturbance-succession pathways (Andela et al., 2017; Jones et al., 2020). Crucially, to clarify the "fire-climate-vegetation" nexus, it is necessary to mechanistically understand the following issues: the threshold dynamics

of the relationship between fuel moisture and ignition, the positive feedback loops between pyrogenic emissions and climate warming and vegetation adaptation strategies under changing fire return intervals. This knowledge framework lays the scientific foundation for developing "climate-resilient forest management protocols" for boreal forest ecosystems.

The Altai-Sayan region lies at the junction of Arid Central Asia and the boreal forest ecosystems. This region features an extremely steep hydrothermal gradient ranging from warm, arid steppes/shrublands in the south to cold, humid closed-canopy boreal forests in the north, forming a vast and sensitive ecotone (Xinjiang Comprehensive Investigation Team, CAS, 1978). It is precisely this "marginal" and "transitional" nature that makes it a natural laboratory and early warning system for studying fire-climate interactions (Fu et al., 2013; Liu et al., 2021). The convergence of two key flammability drivers–coniferous vegetation (*Pinus sibirica* dominance >60%) and intensifying drought regimes has created a pyrogeographic hotspot. This synergy amplifies fire return intervals by 2.3× compared to pre-1990 baselines, fundamentally altering successional pathways and threatening ecological security thresholds (Goldammer & Furyaev, 2013). Remote sensing analyses document a quadrupling of fire events from 712±89 yr^{-1} (1980-2000) to 3024±214 yr^{-1} (2001-2020) with burned area expanding exponentially (R^2=0.91, $p<0.001$) (Ponomarev & Kharuk, 2016), which has a phase coincidence with the dynamics of mean temperatures and climate dryness (Ponomarev & Kharuk, 2016). In the southern Altai, the reduced burned area since 1987 can be attributed to increased moisture and greatly increased investment in fire prevention (Shi et al., 2021). The dynamic changes of fires in the instrumental measurement period driven by human activities and natural processes exhibit distinct differences. However, contemporary observations remain circumscribed by the temporal resolution limitations of satellite archives (post-1980) and instrumental records, creating a <50-year observational window that inadequately captures decadal-scale fire-climate-human feedbacks (Shi et al., 2021; Ponomarev & Kharuk, 2016; Albrich et al., 2018; Kharuk et al., 2021).

Paleoecological approaches spanning centennial to millennial timescales provide

crucial temporal dimensional support for disentangling the complex interactions through pattern-process analysis. Existing Holocene fire records in the Altai-Sayan region have generally established a robust methodological framework for reconstructing fire-vegetation-climate couplings (e.g., Blyakharchuk et al., 2004, 2007, 2008; Hu et al., 2025; Li et al., 2024). However, two critical knowledge gaps remain to be addressed: (1) the complete fire history sequence in western Mongolia, and (2) the spatiotemporal linkages between fire history in this region and montane ecosystem dynamics across the Altai-Sayan ecoregion. To address this issue, this study selected Achit Nuur as the study site because of its continuous and stable depositional environment. Three critical research dimensions include in this study: (1) Reconstructing fire variability during the Holocene interval (~11750-0 cal. yr BP)via the analysis of charcoal in Achit Nuur; (2) Identifying ecotonal heterogeneity in fire regimes through comparison with other already-published paleofire records (n=23) in the nearby regions; (3) Evaluating how dominant tree genera (*Abies, Betula*, *Larix*, *Picea*, *P. sibirica*, *P. sylvestris*) and their summed percentages as forest cover modulate fire characteristics across vegetation types. This study firstly clarifies the long-timescale fire history in the Altai-Sayan ecoregion, as well as its complex associations with climate fluctuations, vegetation succession and human activities. These outputs provide empirical foundations for developing climate-responsive fire management strategies in the Central Asian ecosystems under the future scenarios.

2. Physiographic Settings

2.1. The Altai-Sayan Mountains

The Altai-Sayan Mountains, one of the most prominent mountain ranges in Central Asia, connect with the Kazakhstan Hills to the west, border the Southern Siberian Plain to the north, and adjoin the Junggar Basin-Khangai Mountains to the south (Fig. 1; Feng et al., 2017). Climatologically, this region holds great significance, as it likely served as a transitional zone where Westerlies-dominated climates from the west interacted with Asian Monsoon-influenced climates from the east during the Holocene (Blyakharchuk et al., 2004, 2008; Zhang & Zhang, 2025). Culturally, it also functioned as a cultural crossroads between Asian and European civilizations along

the "Eurasian Steppe Silk Road" (Blyakharchuk & Chernova, 2013; Xiang et al., 2023).

The North Atlantic Oscillation and Siberian anticyclone drive the southward displacement of the westerlies, which transport water vapor from the Mediterranean, Caspian, and Black Seas into the study region during winter and spring (Aizen et al., 2001; Kutzbach et al., 2014). In contrast, the interaction between the Asian Low and Azores High regulates the northward shift of the westerlies, facilitating water vapor transport in summer and autumn (Aizen et al., 2001). These latitudinal shifts of the westerlies induce a southward gradient of decreasing precipitation and increasing climatic aridity, which in turn shapes the characteristic vegetation distribution patterns across Central Asia (Fig. 1). Zonally, vegetation distribution exhibits a strong latitudinal dependence. Specifically, coniferous forests dominate the southern Siberian Plain, while the eastern Kazakhstan Hills and western Mongolia are characterized by steppe ecosystems, and the Junggar Basin is covered by desert-steppe (Chen, 2010). Additionally, the region's vegetation displays distinct vertical zonation with communities transitioning from desert and steppe at lower elevations to forest and alpine meadow at higher elevations (Blyakharchuk & Chernova, 2013; Zhang et al., 2020).

2.2. Achit Nuur

Achit Nuur (49.42°N, 90.52°E; 1444 m a.s.l.) occupies an intermountain basin bounded by the Mongolian Altai to the west, Mungen Taiga Mountain to the north and Kharkhiraa Turgen Mountain to the east (site 1 in Fig. 1) (Sun et al., 2013). The lake exhibits distinct shoreline zonation: low-lying northern/southern margins is salt-marsh vegetation, while elevated eastern and western shores are dominated by desert steppe communities (Sun et al., 2013). Regional vegetation comprises a mosaic of *Stipa krylovii*, *Stipa gobica* and *Cleistogenes soongorica* grasslands interspersed with subshrubs including *Artemisia frigida*, *A. xerophytica*, *A. caespitosa*, *Tanacetum sibiricum*, *T. achillaeoides* and *T. trifidum*. Mountainous areas of the Mongolian Altai host taiga forests dominated by *Larix sibirica* and *P. sibirica* with an understory of *Rosa acicularis* and *Betula rotundifolia* (Sun et al., 2013).

A 2-m sediment core was retrieved from the central lake basin in 2010 using a Livingston-type piston corer (Sun et al., 2013). Five lithological units were identified based on organic matter (OM) content and mean size characteristics (Fig. 2A). Ten bulk samples underwent accelerator mass spectrometry (AMS) ^{14}C dating at the University of Arizona NSF-AMS Facility (Fig. 2A). A 2100-year reservoir correction was applied to all radiocarbon ages prior to calibration due to old carbon-influenced 2099 ^{14}C BP on the surface sediment (Sun et al., 2013). Calibration to calendar years before present (cal. yr BP, relative to 1950 CE) utilized the IntCal20 curve (Reimer et al., 2020). The Bayesian age-depth model was reconstructed using Bacon v2.5.3 (Blaauw & Christen, 2011) (Fig. 2B). This study just focused on the Holocene interval (i.e., the past ~11,750 cal. yr BP).

2.3. Other study sites in the Altai-Sayan Mountains and adjacent plains

Total 24 sites including Achit Nuur (Table 1) were selected to investigate the spatial heterogeneities of fire regimes in the Altai-Sayan Mountains and adjacent plains. These sites were divided into seven regions based on the vegetation distribution and geographic location.

Southeastern/western Altai Mountains within steppe zone (Region A, n=4): Tolbo Lake (site 2; 48.55°N, 90.05°E, 2080 m a.s.l.) is an alpine lake of glacial origin covered by mountain steppe in the Mongolian Altai (Hu et al., 2024). Alahake Lake (site 3; 47.69°N, 87.54°E, 483 m a.s.l.) is located in the Irtysh river valley in the southern Altai Mountains (Li et al., 2019). Kuchuk Lake (site 4; 52.69ºN, 79.84ºE, 98 m a.s.l.) is the largest endorheic basin in Kulunda Basin within the southern Siberia (Rudaya et al., 2020).

Low-relief west Siberian plain (Region B, n=4): Rybnaya Mire (site 5; 57.28ºN, 84.49ºE) is located near the Rybnaya river in the southern taiga of Western Siberia (Feurdean et al., 2022). Plotnikovo Mire (site 6; 56.88ºN, 83.30ºE, 120 m a.s.l) is an ombrotrophic bog located at the eastern margins of the Great Vasyugan Mire on the Western Siberia (Feurdean et al., 2020). Shchuchye Lake (site 7; 57.13ºN, 84.61ºE, 80 m a. s. l.) is located in the south taiga zone of West Siberian plain (Blyakharchuk et al., 2024). Ulukh–Chayakh Mire (site 8; 57.34ºN, 88.32ºE) located on a terrace of the

Chulym river in the southern taiga of Western Siberia (Feurdean et al., 2022).

Northern Altai Mountains (Region C, n=4): Chudnoye Lake (site 9; 54.03ºN, 89.01ºE, 1147 m a.s.l.), Tundra Mire (site 10; 53.79ºN, 88.27ºE, 247 m a.s.l.) and Kuatang Mire (site 12; 51.81ºN, 87.32ºE, 650 m a.s.l.) are located in the northern Altai Mountains in areas covered by wet mountain dark coniferous (with *Abies, Pinus sibirica* and *Betula*) taiga (Blyakharchuk, 2022; Blyakharchuk et al., 2024). Mokhovoe Bog (site 11; 52.52ºN, 86.42ºE, 283 m a.s.l.) is located on western piedmont of north Altai covered by birch (with *Betula pendula+Betula pubescens*) and pine (*Pinus sylvestris*) forest-steppe (Blyakharchuk, 2022).

Central Altai Mountains within the forest zone (Region D, n=3): Dzhangyskol Lake (site 13; 50.18°N, 87.73°E, 1800 m a.s.l.) is situated in the western Kurai intermontane depression covered with steppe vegetation and bounded by small hills with *Pinus sibirica* and *Larix sibirica* (Blyakharchuk et al., 2008). Two freshwater lakes are situated 1.5-4 km apart at different elevations below the timberline in the Ulagan Plateau: Uzunkol Lake (site 14; 50.48°N, 87.1°E, 1985 m a.s.l.) and Kendegelukol Lake (site 15; 50.50°N, 87.63°E, 2050 m a.s.l.) (Blyakharchuk et al., 2004).

Central Altai Mountains above the forest limit (Region D, n=3): Tashkol Lake (site 16; 50.45°N, 87.67°E, 2150 m) lies at the timberline (upper limit of continuous forest) of Ulagan Plateau in the central Altai part of Russian Altai (Blyakharchuk et al., 2004). Akkol Lake (site 17; 50.25°N 89.62°E, 2204 m a.s.l.) and Grusha Lake (site 18; 50.38°N, 89.42°E, 2413 m a.s.l.) are situated in the western Karginskaya high-mountain depression near the junction of the Chikhachev and Shapshal ranges of the south-eastern part of the Russian Altai Mountains (Blyakharchuk et al., 2007).

Western Sayan Mountains (2000-2700 m a.s.l.) (Region F, n=3): Buibinskoye Mire (site 19; 52.84°N, 93.52°E, 1377 m a.s.l.) and Bezrybnoye Mire (site 20; 52.81ºN, 93.50ºE, 1395 m a.s.l.) are located in the Yergaki Nature Reserve (Blyakharchuk et al., 2022). Lugovoe mire (site 21; 52.85ºN, 93.35ºE, 1299 m a.s.l.) is the largest mire in the Yergaki Natural Park with the largest hydrological catchment in the Western Sayan Mountains (Blyakharchuk and Chernova, 2013).

Khangai Mountains (peaks 4031 m a.s.l.) (Region G, n=3): Three selected sites include Olgi Lake (site 22; 48.32°N, 98.01°E, 2012 m a.s.l.) (Unkelbach et al., 2021), Shireet Naiman Nuur (site 23; 46.53°N, 101.82°E, 2429 m a.s.l.) (Barhoumi et al., 2024) and Ugii Nuur (site 24; 47.77°N, 102.78°E, 1330 m a.s.l.) (Wang et al., 2011).

3. Methods

3.1. Charcoal analysis

The pre-treatment process for charcoal analyses involved the standard pollen extraction method (Tang et al., 2022; Wang et al., 2020). Charcoal particles were identified using a light microscope, characterized by dark black color, opaque appearance, sharp corners, and straight edges. The treated samples were prepared into moving pieces by adding an appropriate amount of glycerin using particle counting method, which were then observed and counted under Lycra microscope. A total of more than 300 grains of all sizes were counted and the quantity of Lycopodium spores was determined for each sample. The concentration of charcoal was then calculated based on the statistical data (Li et al., 2010): W=A*n/(N*G), Where W is the charcoal concentration (particles/g), A is the statistical number of charcoal fragments, n is the number of additional lycopodium spores, N is the statistical number of lycopodium spores, and G is the sample weight (g). Charcoal influx (CHAR, particles/cm^2/yr) is their respective concentration dividing by the sediment rate (yr/cm).

3.2. Generalized additive models

Generalized additive models (GAMs) employ a link function to examine the relationship between the mean of the response variable (i.e., dependent variable) and a smoothed function of the predictor variable (i.e., independent variable). In this study, we investigated the associations between charcoal influx and two types of predictors: (1) individual taxa, including *Abies, Betula, Larix, Picea, P. sibirica,* and *P. sylvestris*; and (2) total forest cover, defined as the summed percentage of the aforementioned six taxa. We constructed GAMs with a quasi-Poisson distribution and a log link function using the mgcv package in R (Wood, 2017). This distribution was selected because it flexibly corrects for overdispersion by incorporating a dispersion parameter, eliminating the need for additional assumptions regarding the probability distribution

of the data (Wood, 2017). For all smoothing terms, we used thin-plate splines as the basis function—this is the default setting in the gam() function of the mgcv package. Model fitting was performed via restricted maximum likelihood (REML) for smoothness selection.

3.3. Data processing for comparison

To standardize charcoal influx for comparison, three-step process was employed to calculate Z-scores (Power et al., 2007):

(1) Mini-max transformation:

$$C_i^{'} = (C_i - C_{min})/(C_{max} - C_{min})$$

In this expression, $C_i^{'}$ is the value of mini-max transformed for the i-th sample at each sequence, C_i is RoCs of the i-th sample at each sequence, C_{max} is the maximum value of C_i, and C_{min} is the minimum value of C_i.

(2) Box-Cox transformation for homogenization of variance:

$$C_i^{*} = \begin{cases} ((C_i^{'} + \alpha)^{\lambda} - 1)/\lambda, \lambda \neq 0 \\ log(C_i^{'} + \alpha), \lambda = 0 \end{cases}$$

In this expression, C_i^{*} is the Box-Cox value transformed for $C_i^{'}$, λ is the parameter of Box-Cox transformation estimated using maximum likelihood, and α is a small positive constant (0.01 in this study) used to ensure that both $C_i^{'}$ and λ are zero.

(3) Z-score calculation:

$$Z - \text{score} = (C_i^{*} - \overline{C_i^{*}})/\delta$$

In this expression, $\overline{C_i^{*}}$ is the average value of C_i^{*} and δ is the standard deviation of C_i^{*}.

Since the sample resolution at most study sites is approximately 200 years, a 200-year time slice was selected to perform linear interpolation on the transformed charcoal Z-scores. Subsequently, the interpolated data were averaged to characterize the charcoal influx conditions across different regions. The Holocene interval was divided into three intervals: early Holocene (~11.75-~8.2 cal. kyr BP), middle Holocene (~8.2-~4.2 cal. kyr BP) and late Holocene (~4.2-~0 cal. kyr BP) (Marcott et al., 2013).

4. Results and Discussions

4.1. Reconstructed fire history and its relationship with vegetation at Achit Nuur

The charcoal influx in Achit Nuur varies from 2643.46 to 76.43 particles/cm^2/yr with an average of 509.99 particles/cm^2/yr. Higher charcoal influx has been recorded since ~2 cal. kyr BP with the maximum occurring during the interval of ~1.2-~0.79 cal. kyr BP (Fig. 3a). For pollen percentages of key taxa: *P. sibirica*, *Betula* and *Picea* exhibited a rapid increasing trend before ~6 cal. kyr BP, followed by a gradual decreasing trend thereafter (Fig. 3b) (Sun et al., 2013). High *Larix* pollen content was observed at ~6–~2 cal. kyr BP, while *Abies* pollen remained relatively low throughout the entire sediment sequence. GAMs analyses reveal charcoal influx is significantly positively correlated with increasing *Betula* ($p=0.02$), *P. sibirica* ($p=0.001$) and total forest cover ($p<0.001$); in contrast, it is significantly positively correlated with decreasing *Larix* ($p<0.001$) and *Picea* ($p=0.001$) abundances (Table 2, Fig. 1). This pattern can be mechanistically explained by the differing combustibility of vegetation taxa: *Betula* and *P. sibirica* have higher fuel flammability (e.g., thinner bark, more resinous tissues) that promotes fire spread and intensity, while *Larix* and *Picea* (especially mature individuals) have lower flammability (e.g., thicker bark, less volatile compounds) or form dense canopies that reduce surface fuel drying (Feurdean et al., 2020, 2022)—thus, shifts in their relative abundances directly regulate the frequency and severity of fires, which is reflected in the variation of charcoal influx.

4.2. Holocene climate-fuel feedbacks across the selected different sites

4.2.1. Southeastern/western Altai Mountains within the steppe zone (Region A):

Charcoal records from four lacustrine systems (Achit Nuur, Tolbo, Alahake and Kuchuk Lakes) reveal a consistent amplification of fire activities during the late-Holocene (Fig. 4b), with distinct peak intervals observed across sites: ~1.2-~0.79 cal. kyr BP in Achit Nuur, ~1.20-~0.65 cal. kyr BP in Tolbo Lake, ~1.44-~1.02 cal. kyr BP in Alahake Lake and a pronounced doubling of charcoal flux over the past two millennia in Kuchuk Lake. Pollen spectra further highlight ecosystem-specific fuel configurations that underpin these fire patterns: Tolbo Lake is dominated by an alpine steppe ecosystem (*Artemisia*-Poaceae), where herbaceous plants serve as the primary surface fuel; Achit Nuur features montane *P. sibirica*, with resinous coniferous tissues

providing highly flammable fuel sources; and Alahake Lake supports lowland *Picea-Larix* mixed forest, where leaf litter and understory vegetation contribute to fuel loads (Sun et al., 2013; Hu et al., 2024; Li et al., 2021; Rudaya et al., 2020).

This divergence in fuel type directly explains why fire responses to environmental changes vary across lakes. GAMs results confirm that charcoal influx in Achit Nuur and Tolbo Lake is primarily controlled by forest cover (Table 2, Fig. S1). Specifically, *Larix* (accounting for 41.9% of the explanatory power) and *P. sibirica* (34.5%) are the key drivers of charcoal influx in Achit Nuur, while *P. sibirica* (13.3%) plays a dominant role in Tolbo Lake. In Alahake Lake, birch trees (with their thin bark and volatile leaf litter) are identified as the main combustion source, whereas in Kuchuk Lake, the primary fuels are *Betula* and *P. sylvestris* forest—both of which have high ignition potential (Table 2, Fig. S2).

4.2.2. West Siberian plain (Region B, n=4):

Rybnaya Mire is located on the low terrace of the Ob' River (83 m a.s.l.), with vegetation dominated by *P. sylvestris* and *Betula*. Its charcoal record shows higher influx during the middle Holocene, with no significant charcoal pulse over the past 50 years (Feurdean et al., 2020) (Fig. 4c). GAM analysis reveals that fire activity is primarily controlled by coniferous vegetation: *Picea* cover explains 44.5% of the variance in charcoal influx, while *Betula* contributes 18.4% (Table 2, Fig. S2). Charcoal influx in Plotnikovo Mire shows a rapid increase since ~2 cal. kyr BP (Feurdean et al., 2020), with forest cover explaining 39.7% of the deviance in charcoal influx (Table 2, Fig. S2). The post-2 cal. kyr BP surge in charcoal is likely linked to the gradual expansion of *Betula*—this species produces resinous bark that are highly flammable, and as its cover increased, the accumulation of combustible fuel accelerated, creating more favorable conditions for fire ignition and spread (Feurdean et al., 2022). Shchuchye Lake exhibits a phased fire regime, with a strong charcoal pulse at ~12-~11 cal. kyr BP and slightly increased fire activity during the late Holocene (Fig. 4c). Ulukh-Chayakh Mire records key fire events in the last millennium and during the ~4.5-~3 cal. kyr BP interval (Fig. 4c).

GAM analysis reveals divergent fire-vegetation relationships across sites (Table

2, Fig. S2 and S3), rooted in differences in canopy cover and associated fuel microenvironments: (1) Negative correlation at Rybnaya and Plotnikovo Mires (canopy cover >75%): Dense canopies reduce understory light availability, maintaining high microclimatic humidity and limiting the growth of herbaceous understory fuels. Humid conditions keep surface fuels moist, while sparse understory fuels reduce fire intensity and spread — together, these factors create an inverse relationship between canopy cover and charcoal influx. (2) Positive correlation at Shchuchye Lake (canopy cover <65%): Open canopy structures allow more solar radiation to reach the understory, promoting the growth of flammable grassy undergrowth. Grasses dry out quickly and ignite easily, serving as ignition fuels that trigger larger fires; the open environment also facilitates air circulation, which accelerates fire spread—these factors lead to a positive association between canopy openness (and associated grassy fuels) and charcoal influx.

4.2.3. Northern Altai Mountains (Region C, n=4):

Chudnoye Mire is situated in a remote mountain taiga near the upper forest limit (Fig. 1). Its charcoal record exhibits a distinct temporal pattern: a decline in influx during the early to mid-Holocene, followed by intensification in the late Holocene (Fig. 4d). Its variations often correspond to shifts in dominant tree species within mountain forests—this is evident in the positive correlation between charcoal influx and pollen abundances of *Betula* (30.3%) and *Picea* (20.5%) (Table 2, Fig. S3). The mechanism underlying this correlation lies in fuel properties of these conifers: *Betula* and *Picea* produce needle litter and resinous tissues that are highly flammable when dry, so their expansion increases fuel availability, directly boosting fire frequency and intensity (Blyakharchuk et al., 2024).

Tundra Mire is characterized by dense forests of *Abies* and *Betula*, as reflected in its pollen assemblage. Its charcoal influx showed a decreasing trend before ~4 cal. kyr BP, after which it began to rise. GAM analysis reveals that the changes in fire activities likely stems from *Larix*'s fire-loving traits (22.7%) (Table 2, Fig. S4). Mokhovoe Bog covered by a birch forest-steppe ecosystem records four charcoal influx peaks at ~11.5–~9.5, ~8.5–~7, ~5.6–~4 and ~1.5–~1 cal. kyr BP. The only

statistical correlation (11.9%) observed here is between *Picea* pollen and charcoal influx (Table 2, Fig. S4), which can be mechanistically explained by climatic controls on fuel production: a more humid climate enhances landscape bioproductivity, promoting *Picea* growth and increasing the accumulation of flammable needle litter—even though *Picea* is less flammable than *Betula*, the sheer increase in fuel quantity outweighs its low flammability, driving higher charcoal influx (Blyakharchuk, 2022).

Its charcoal influx in Kuatang Lake has shown a clear increase between ~3.5 and ~2 cal. kyr BP, followed by a subsequent decline (Fig. 4d, Fig. S4). A key pattern emerges in its vegetation-fire relationships: a positive correlation between charcoal influx and *Betula* pollen, contrasted with negative correlations with *Abies*, *P. sibirica* and *P. sylvestris*. This suggests that the post-3.5 cal. kyr BP charcoal increase is primarily driven by *Betula* expansion—*Betula* has thin, volatile bark and fast-drying leaf litter that ignite easily, whereas *Abies* and the two pine species have thicker bark or dense canopies that inhibit fire; thus, a shift toward *Betula*-dominated vegetation directly elevates fire activity and charcoal deposition (Blyakharchuk et al., 2024).

4.2.4. Central Altai Mountains within the forest zone (Region D, n=3):

Holocene charcoal influx exhibited a consistent increasing trend in Kendegelukol Lake, Uzunkol Lake and Dzhangyskol Lake (Fig. 4e), with a notably pronounced acceleration during the late Holocene. Specifically, Uzunkol Lake saw a particularly sharp rise in charcoal influx starting at ~1.2 cal. kyr BP, while Dzhangyskol Lake recorded a marked increase from ~0.5 cal. kyr BP onward. Notably, Uzunkol Lake documented elevated charcoal influx between ~9.5 and ~9 cal. kyr BP, a period that coincided with the regional landscape transition from a steppe-dominated to a forest-dominated system (Blyakharchuk et al., 2008). However, charcoal influx failed to sustain these high levels following the transition—a pattern rooted in shifting fire regime stability. The anomalous charcoal peak at ~9.5-~9 cal. kyr BP likely arose from an unstable fire regime during the initial establishment of forests: the prevailing dry climate at this time accelerated fuel desiccation, while the expansion of trees and shrubs substantially increased combustible fuel availability. This combination of dry

conditions and abundant fuel made the nascent forest ecosystem highly susceptible to ignition, driving frequent, intense fires and thus high charcoal deposition (Blyakharchuk & Pupysheva, 2022). After the landscape stabilized as mature forest, charcoal influx at Uzunkol Lake declined—a shift indicative of a transition to a more humid climate (Zhang and Zhang, 2025). Humid conditions reduced fuel dryness and promoted the development of dense forest canopies, which further suppressed fire spread by maintaining cool, moist understory microclimates and slowing litter decomposition (Blyakharchuk et al., 2004).

In contrast, Kendegelukol Lake and Dzhangyskol Lake exhibited only modest increases in charcoal influx throughout the Holocene (Fig. 4e). This discrepancy highlights Uzunkol Lake's greater sensitivity to local fire activity, a trait linked to its location within the forest-steppe transition zone (Blyakharchuk et al., 2004). As an ecotone, this region is characterized by a dynamic mix of steppe herbs and forest woody plants—vegetation that is inherently responsive to small changes in climate (e.g., precipitation or temperature shifts). Even minor climatic fluctuations can alter the balance between herbaceous and woody fuels, directly modifying fuel flammability and accumulation rates, and thus amplifying fire responses. In contrast, Kendegelukol Lake and Dzhangyskol Lake are situated in more homogeneous vegetation zones (i.e., closed forests), where stable plant communities buffer against small-scale environmental changes, leading to more muted fire activity signals. This observation aligns with prior research, which has shown that forest-wooded grassland ecotones were disproportionately sensitive to Holocene climate variability compared to single-vegetation zones (Lezine et al., 2023).

GAMs analysis reveals strong positive correlations between charcoal influx and the pollen abundances of *Abies*, *Betula* and *P. sylvestris* across all three lakes (Table 2, Fig. S5). This relationship underscores a key mechanistic link: late-Holocene forest expansion enhanced the accumulation of fuel loads, which in turn drove shifts in fire regimes. Specifically, *Abies* and *P. sylvestris* produce resin-rich needles that are highly flammable when dry, while *Betula* has thin, volatile bark and fast-drying leaf litter—all of which serve as high-quality fuels. As these tree species expanded, their

accumulated biomass increased both the quantity and flammability of available fuel, lowering the threshold for ignition and increasing fire frequency and intensity, which are recorded as higher charcoal influx.

4.2.5. Central Altai Mountains above the forest limit (Region E, n=3):

Tashkol Lake is situated above the modern forest limit at 2150 m a.s.l. and was covered by glacial ice during the last glacial period (Blyakharchuk et al., 2004). A sharp peak in charcoal influx at ~11–~10.5 cal. kyr BP is most likely caused by the redeposition of pre-existing microcharcoal by glacial meltwaters (Blyakharchuk et al., 2004). This mechanism involves meltwater eroding Pleistocene-aged charcoal from surrounding glaciated terrain and transporting it into the lake basin, creating a transient charcoal peak unrelated to contemporary fire regimes (Blyakharchuk et al., 2024). Subsequently, between ~10.5 and ~4 cal. kyr BP, the expansion of forested landscapes in the central Altai—coupled with middle Holocene warming—left a clear imprint on Tashkol Lake's charcoal influx patterns. This link underscores a climate-dependent mechanism: warmer, wetter conditions during the mid-Holocene enhanced high-elevation bioproductivity, promoting the growth of *Picea* and other woody vegetation; this increased fuel availability supported more frequent fires, translating to higher charcoal influx. In contrast, late Holocene cooling reduced vegetation growth and fuel accumulation, leading to lower fire activity and declining charcoal influx—highlighting how temperature regulates fuel production and fire regimes in alpine environments.

Grusha Lake, located at an even higher elevation (2413 m a.s.l.), also experienced glacial coverage during the last glaciation (Rudoy and Yatsuk, 1986). An exceptionally high charcoal influx during the late glacial period (~12-~11 cal. kyr BP) is attributed to the allochthonous (externally sourced) redeposition of ancient charcoal (Blyakharchuk et al., 2024). Following deglaciation (~10.5 cal. kyr BP), the previously ice-covered, bare terrain surrounding Grusha Lake became colonized by vegetation (Blyakharchuk et al., 2004). This vegetative cover stabilized the landscape, reducing soil erosion and limiting the transport of ancient charcoal into the lake; consequently, the redeposition of microcharcoal declined sharply, and charcoal influx

shifted to reflect in-situ fire activity driven by local fuel availability.

Akkol Lake exhibits an overall charcoal influx trend similar to that of Grusha Lake, with one critical exception: it lacks the ~12–~11 cal. kyr BP charcoal peak. This discrepancy is directly explained by Akkol Lake's lower elevation, which spared it from glacial coverage during the last glaciation (Blyakharchuk et al., 2007). Without glacial to accumulate and later release ancient microcharcoal via meltwater, there was no source for the allochthonous charcoal spike observed in Grusha Lake. Additionally, the lake's lower-elevation setting maintained drier conditions during the late glacial period, which inhibited the transport of sediment and charcoal from surrounding areas—further preventing the formation of a charcoal peak. Instead, Akkol Lake's charcoal record from this period reflects only minimal in-situ fire activity, consistent with its dry, unglaciated environment and limited fuel availability.

GAMs further identify the key vegetation sources of biomass combustion across three lakes: *Picea* in Tashkol Lake; a combination of *Picea* and *P. sylvestris* in Akkol Lake; and *Larix* and *Picea* in Grusha Lake (Table 2, Fig. S6). These species-specific associations reflect differences in fuel flammability — for instance, *Larix* and *P. sylvestris* produce resin-rich needles and bark that ignite easily, while *Picea* litter, though less flammable, contributes to fuel loads when accumulated in large quantities — ultimately driving lake-specific variations in charcoal influx. Notably, significant differences in charcoal influx magnitudes and timing were observed among three lakes, largely tied to their distinct elevations, glacial histories and post-glacial vegetation development.

4.2.6. Western Sayan Mountains (Region F, n=3):

Three peat cores-Lugovoe Peat, Bezrybnoye Mire and Buibinskoye Mire-exhibited a consistent decreasing trend in charcoal influx throughout the Holocene, with one notable exception: Buibinskoye Mire recorded a distinct charcoal influx peak around ~12–~11 cal. kyr BP (Fig. 4g). During the late glacial and early Holocene, permafrost was likely widespread in the soil profiles of the Western Sayan region (Blyakharchuk et al., 2022), creating waterlogged, nutrient-poor soil conditions that restricted vegetation growth—only *Picea*, a species adapted to cold, waterlogged

environments, could thrive under these constraints (Blyakharchuk et al., 2013, 2022). As the climate warmed and permafrost receded, soil drainage improved and nutrient availability increased, favoring the establishment of *P. sibirica* and *Abies* over *Picea* (Blyakharchuk et al., 2013, 2022). This vegetation shift had profound implications for fire regimes: at ~11 cal. kyr BP, the onset of forestation (marked by the expansion of *P. sibirica* and *Abies*) led to an increase in charcoal influx, as the newly established woody vegetation provided a steady supply of combustible fuel. Notably, just prior to this forestation event (~11.5-~11 cal. kyr BP), intense fires devastated the existing *Picea* forests—likely triggered by a transient period of warming that dried the sparse *Picea* litter, making it vulnerable to ignition despite the region's generally cold conditions. Between ~10.5 and ~7 cal. kyr BP, charcoal influx increased in Buibinskoye Mire, followed by a gradual decline in the late Holocene. The mid-Holocene warming drove this transient charcoal increase: warmer temperatures enhanced the growth of woody vegetation and increased the accumulation of flammable fuel (e.g., leaf litter, dead branches) in the western Sayan Mountains (Blyakharchuk et al., 2013, 2022). After ~7 cal. kyr BP, the cooling temperatures reduced forest bioproductivity and slowing fuel accumulation both suppressed fire frequency and intensity, leading to a gradual decline in charcoal influx across three sites.

GAMs results highlight species-specific roles in driving charcoal influx: in Lugovoe Peat, *Abies* and *Larix* are the primary contributor to charcoal production—*Larix*'s resin-rich needles and *Abies*'s dense, flammable litter together fuel intense fires; in Buibinskoye Mire, *Abies* also plays a significant role in driving charcoal influx (Table 2, Fig. S7). Notably, no significant statistical relationship was found between charcoal influx and vegetation in Bezrybnoye Mire. However, *P. sylvestris* -a well-documented fire-resistant species (Feurdean et al., 2022)-accounted for the largest proportion of deviance explanation (28.10%) for charcoal influx at this site (Table 2). This pattern suggests a mechanistic link: the expansion of *P. sylvestris* forests reduces the area covered by more flammable species (e.g., *Abies*, *Larix*), thereby decreasing the availability of high-quality fuel. Support for this comes from

the negative correlation observed in Lugovoe Peat and Buibinskoye Mire between *P. sylvestris* spread and declining biomass combustion. Over time, the increasing dominance of fire-resistant *P. sylvestris* has reduced the overall flammability of forest ecosystems, contributing to the long-term decline in charcoal influx observed across the forested areas.

4.2.7. Khangai Mountains (Region G, n=3):

GAMs analysis revealed a negative correlation between charcoal influx and both forest cover and other woody types in Olgi Lake (Table 2, Fig. S8). This pattern strongly suggests that charcoal influx in Olgi Lake is primarily controlled by herbaceous-dominated steppe vegetation—a mechanistic link rooted in fuel properties. An decrease in forest cover would promote grass-fueled fires, leading to higher charcoal influx—explaining the observed negative correlation. In contrast, charcoal influx in Shireet Naiman Nuur and Ugii Nuur showed a positive correlation with forest cover (Table 2, Fig. S8). This indicates that fire activity in these two lakes is mainly regulated by woody vegetation, with *P. sibirica* exhibiting the highest explanatory power for charcoal influx. The dominance of *P. sibirica* as a driver reflects its unique fuel characteristics: it produces resin-rich needles and bark that are highly combustible, and its litter accumulates quickly on the forest floor, providing a continuous supply of dry fuel. The striking differences in charcoal-vegetation relationships among three lakes can be attributed to their distinct vegetation distributions, which are tightly linked to elevation-driven climate gradients.

Although Shireet Naiman Nuur recorded a gradual decline in charcoal influx during the middle-to-late Holocene, its overall charcoal influx remained considerably lower than that of Olgi Lake and Ugii Nuur (Fig. 4h). This discrepancy is explained by low vegetation cover at Shireet Naiman Nuur: even with forest presence, cooler temperature and shorter growing seasons at its high elevation limit overall bioproductivity, resulting in limited fuel accumulation (Barhoumi et al., 2024). Notably, Olgi Lake and Ugii Nuur recorded higher charcoal influxes during specific intervals: ~3.4–~3.1 cal. kyr BP at Olgi Lake and ~2.4–~2.1 cal. kyr BP at Ugii Nuur. These spikes are likely driven by local drought conditions, a conclusion supported by

the limited human impact documented during these periods (Unkelbach et al., 2021; Barhoumi et al., 2024; Wang and Feng, 2013). Drought acts as a key fire catalyst by reducing fuel moisture content: even in Olgi Lake's steppe (where grasses are the main fuel) or Ugii Nuur's forests (where woody litter dominates), dry conditions make fuels more susceptible to ignition by natural sources (e.g., lightning). Without significant human interference to alter fire regimes, these drought-induced fuel dryness events would directly trigger increased fire activity, leaving a clear signal of higher charcoal concentrations in the sediment record.

4.3. Holocene climate-fuel feedbacks across the different regions

In Region A, synthesized charcoal influx indicate that fire activity was suppressed during the early Holocene-a pattern linked to moisture-limited vegetation productivity (Zhang and Zhang, 2025). Specifically, low precipitation restricted the growth of both herbaceous and woody plants (Sun et al., 2013; Hu et al., 2024; Li et al., 2021; Rudaya et al., 2020), resulting in insufficient fuel to sustain frequent or intense fires. From the mid-Holocene to ~2 cal. kyr BP, increased precipitation (Hu et al., 2024; Zhang and Zhang, 2025) facilitated the expansion of vegetation cover, tripling the consistent increasing fire activities (Sun et al., 2013). Notably, after ~2 cal. kyr BP, anomalous charcoal influx peaks across all four sites likely correlate with markers of agriculture expansion indicated by an increasing cereal-type *Poaecea* pollen (Xiao et al., 2021). This observation points to a critical ecological shift: human activities, such as intentional burning to expand pastures or clear land for crop cultivation, directly increased fire frequency. These anthropogenic disturbances ultimately overrode the previously dominant climate-driven controls on fuel availability and fire activity (Li et al., 2021; Xiao et al., 2021; Rudaya et al., 2020).

A cross-site synthesis of fire regimes in Region B identifies three distinct phases, each driven by unique environmental and anthropogenic mechanisms: ~12-~11 cal. kyr BP: A charcoal pulse is only recorded at Shchuchye Lake, likely resulting from meltwater-mediated charcoal deposition (Blyakharchuk et al., 2024). ~8.5-~6 cal. kyr BP: Rybnaya Peat exhibits a second phase of higher charcoal influx, linked to two interrelated changes: increased proportion of dark taiga and fire avoiders (e.g., *P.*

sibirica and drier conditions (Feurdean et al., 2022). Past ~2 cal. kyr BP: A widespread increase in fire activity across all sites coincides with two key drivers: regional megadrought conditions (Feurdean et al., 2022; Zhang and Zhang, 2025) and the emergence of fire use by pastoralist communities (Feurdean et al., 2022). Megadrought dried out vegetation, increasing fuel flammability and frequency of natural ignitions; pastoralists intentionally used fire to clear vegetation and expand pastures, further amplifying fire activity, creating a synergistic effect between natural and anthropogenic drivers (Zhang et al., 2022).

Regional synthesis of charcoal influx in Region C reveals two dominant trends: a gradual decline in the early to mid-Holocene, followed by a late-Holocene increase that eventually shifted to a downward trajectory. The former is likely related to temperature-regulated forest vegetation dynamics. The latter is correlated with two synergistic drivers: regional climatic humidification and intensified anthropogenic activities (Blyakharchuk et al., 2023; Zhang and Zhang, 2025). Humidification boosted vegetation growth and fuel accumulation, laying the material foundation for fires; meanwhile, human activities (such as intentional burning for hunting, pasture expansion or settlement) provided ignition sources, amplifying fire frequency beyond natural variability. This feature directly corresponds to numerous archaeological sites of ancient human cultures, indicating densely populated areas (Panyushkina, 2012; Agatova et al., 2014; Xiang et al., 2024). Of particular note, Mokhovoe Bog exhibits the most pronounced charcoal fluxes—this reflects persistent human occupation of its resource-rich forest-steppe landscape since the Mesolithic era (Blyakharchuk, 2022), as the bog's proximity to both forest resources and open steppe made it a favorable hub for prehistoric communities. Notably, a Bronze Age charcoal pulse (~4-~3 cal. kyr BP) at Kuatang Bog and an Early Iron Age pulse (~3 cal. kyr BP) at Tundra Mire coincide with the Kuznetski Alatau Mountains—a known center of ancient Siberian metallurgy (Slavnin and Sherstova, 1999).

Regional synthesis of three records in Region D confirms a sustained upward trajectory in charcoal influx throughout the Holocene, with the past two millennia witnessing a 2.3-fold increase relative to early Holocene baselines (Fig. 4e). This

long-term trend reflects the cumulative effects of both natural drivers (e.g., climate-mediated fuel accumulation via forest expansion) and anthropogenic drivers (e.g., pastoral burning and land clearance), which together intensified fire activity across the region over time. Beyond vegetation-driven changes, the anomalous surge in charcoal influx after ~1.0 cal. kyr BP likely reflects the synergistic effects of anthropogenic drivers. Intensified pastoral burning practices (e.g., intentional fire use to clear invasive shrubs and expand grazing lands) directly increased ignition sources (Zhang et al., 2022). Additionally, these human activities altered vegetation structure further amplifying fuel flammability and fire activity (Blyakharchuk et al., 2004, 2008).

Regional integrated Z-scores of charcoal influx in Region E indicate a consistent declining trend before ~2 cal. kyr BP, followed by a rapid increase in the post-2 cal. kyr BP period (Fig. 4f). This temporal pattern is linked to temperature-regulated reductions in forest cover prior to ~2 cal. kyr BP; after ~2 cal. kyr BP, however, charcoal influx dynamics were additionally shaped by human activities (Blyakharchuk et al., 2007). Regional integrated Z-scores of charcoal influx in Region F reveal a consistent declining trend before ~1 cal. kyr BP, followed by a rapid increase in the post-1 cal. kyr BP period (Fig. 4f). All three sites are situated between the upper and lower forest limits, a shared topographic position that fostered similar long-term trends in forest composition and cover throughout the Holocene (Blyakharchuk et al., 2013, 2022). The gradual decrease in charcoal influx is primarily influenced by the response of forest cover to temperature changes. The main forest cover exceeds 80%, indicating that material availability is not a limiting factor for regional charcoal influx. The decline in Holocene biomass in Region F is primarily driven by increasing fire-resistant *P. sylvestris* has reduced the overall flammability of forest ecosystems.

Holocene charcoal influx in Region G can be divided into two distinct phases: a rising trend before the past 2000 years, followed by a gradual decline afterwards (Unkelbach et al., 2021; Barhoumi et al., 2024). The relatively higher charcoal influx at ~4-~2 cal. kyr BP is primarily due to increased drought in the region (Wang and Feng, 2023), which led to a rise in combustible materials. In the later phase, despite

the humid climate (Sun et al., 2013; Hu et al., 2024), the absence of a significant increase in charcoal influx in the Khangai Mountains may be attributed to human grazing activities that have fragmented surface vegetation (Zhang S.J. et al., 2021). This assertion is supported by the studies of modern landscape, where livestock grazing eliminates most of the fuels necessary to sustain a fire (Umbanhowar et al., 2009; Zhang et al., 2022).

In terms of regional differences, the trends and driving factors of charcoal influx vary significantly across regions. In Region A and D, low charcoal influx was observed before 2000 cal. yr BP, but driven by distinct mechanisms: aridity limited vegetation cover, which suppressed fire occurrence in Region A; in Region D, high forest coverage (>70%) at sites like Kendegelukol Lake restricted charcoal influx, while Dzhangyskol Lake—located in the forest-steppe transition zone—exhibited low charcoal influx due to low vegetation productivity. Since 2000 cal. yr BP, charcoal influx has increased rapidly in Region A, B, C and D. This surge is primarily attributed to changes in climatic conditions and intensified human activities (e.g., grazing, settlement). In contrast, the post-2000 cal. yr BP decline in charcoal influx in Region G is linked to surface vegetation fragmentation caused by human grazing. Throughout the Holocene, charcoal influx showed an overall decreasing trend in Region E and F: The former is influenced by temperature-driven changes in forest vegetation cover, while the latter is a result of reduced combustible materials—caused by the expansion of *P. sylvestris*, which squeezed the proportion of highly flammable vegetation. In Region D, charcoal influx gradually decreased during the early to middle Holocene—a trend consistent with that observed in Region E and F, and associated with temperature-regulated forest vegetation dynamics.

5. **Conclusions**

We presents a long-term fire record from the western Mongolia and evaluates the spatial variations in charcoal influx and its relationship with vegetation across the Altai-Sayan Mountains and adjacent plains. Before 2000 cal. yr BP, Regions A and D both had low charcoal influx but for different reasons: aridity limited vegetation cover and suppressed fires in Region A; in Region D, high forest coverage (>70%,

Kendegelukol Lake) restricted charcoal influx, while Dzhangyskol Lake (forest-steppe transition zone) had low influx due to low vegetation productivity. Additionally, Region D saw a gradual decline in charcoal influx during the early to middle Holocene-mirroring trends in Regions E and F, and linked to temperature-regulated forest dynamics. Since 2000 cal. yr BP, Regions A, B, C, and D experienced rapid increases in charcoal influx, driven mainly by climatic changes and intensified human activities. By contrast, Region G had a post-2000 cal. yr BP decline in charcoal influx, may tie to surface vegetation fragmentation from grazing. Across the entire Holocene, Regions E and F showed an overall decreasing trend in charcoal influx: Region E's decline was influenced by temperature-driven changes in forest cover, while Region F's resulted from reduced combustible materials—caused by *P. sylvestris* expansion squeezing out highly flammable vegetation. This research elucidates the long-term relationship between charcoal influx and vegetation composition across different zones in the Altai-Sayan Mountains and adjacent plains, which holds practical significance for predicting and managing future fire dynamics.

CRediT authorship contribution statement

Dongliang Zhang: Writing – review & editing, Validation, Methodology, Funding acquisition, Conceptualization. Blyakharchuk Tatiana, Aizhi Sun, Xiaozhong Huang: Writing – original draft, Visualization, Methodology, Data curation. Yuejing Li – Data curation.

Declaration of Competing Interest

The authors declare that they have no known competing financial interests or personal relationships that could have appeared to influence the work reported in this paper.

Acknowledgment. This research was financially supported by National Natural Science Grants of China (No. 42471183), Youth Innovation Promotion Association of Chinese Academy of Sciences (No. 2022447) and National Natural Science Grants of China (No. 42220104001). We thank anonymous reviewers for their valuable comments, which significantly improved the manuscript.

References

Agatova, A.R., Nepop, R.K., Bronnikova, M.A., Slyusarenko, I.Tu., Orlova, L.A.

698 Human occupation of South Eastern Altai highlands (Russia) in the context of
699 Environmental changes. Archaeological and Anthropological Sciences. DOI
700 10.1007/s12520-014-0202-7.
701 Albrich, K., Rammer, W., Thom, D., Seidl, R., 2018. Trade-offs between temporal
702 stability and level of forest ecosystem services provisioning under climate
703 change. Ecological Applications, 28(7), 1884-1896.
704 Andela, N., Morton, D.C., Giglio, L., Chen, Y., van der Werf, G.R., Kasibhatla, P.S.,
705 DeFries, R.S., Collatz, G.J., Hantson, S., Kloster, S., Bachelet, D., Forrest, M.,
706 Lasslop, G., Li, F., Mangeon, S., Melton, J.R., Yue, C., Randerson, J.T., 2017. A
707 human-driven decline in global burned area. Science, 356, 1356-1362.
708 Archibald, S., Lehmann, C. E., Gómez-Dans, J.L., Bradstock, R.A., 2013. Defining
709 pyromes and global syndromes of fire regimes. PNAS, 110(16), 6442-6447.
710 Barhoumi, C., Bliedtner, M., Zech, R., Behling, H., 2024. Holocene vegetation, fire,
711 climate dynamics and human impact in the upper Orkhon Valley of the Khangai
712 Mountains, Mongolia. Quat. Sci. Rev. 334, 108713.
713 Barhoumi, C., Bliedtner, M., Zech, R., Behling, H., 2024. Holocene vegetation, fire,
714 climate dynamics and human impact in the upper Orkhon Valley of the Khangai
715 Mountains, Mongolia. Quat. Sci. Rev. 334, 108713.
716 Bezrukova, E.V., Abzaeva, A.A., Letunova, P.P., Kulagina, N.V., Vershinin, A.V.,
717 Belov, A.V., Orlova, L.A., Danko, L.V., Krapivina, S.M., 2005. Post-glacial
718 history of Siberian spruce (Picea obovate) in the lake Baikal area and the
719 significance of this species as a paleo-environmental indicator. Quaternary
720 International 136, 47-57. DOI: 10.1016/j.quaint.2004.11.007.
721 Blyakharchuk, T.A., Wright, H.E., Borodavko, P.S., van der Knaap, W.O., Ammann,
722 B., 2004. Late Glacial and Holocene vegetational changes on the Ulagan
723 high-mountain plateau, Altai Mountains, southern Siberia. Palaeogeography,
724 Palaeoclimatology, Palaeoecology, 209(1-4), 259-279.
725 Blyakharchuk, T.A., Wright, H.E., Borodavko, P.S., van der Knaap, W.O., Ammann,
726 B., 2007. Late glacial and Holocene vegetational history of the Altai mountains
727 (southwestern Tuva Republic, Siberia). Palaeogeography, Palaeoclimatology,

728 Palaeoecology, 245(3-4), 518-534.
729 Blyakharchuk, T.A., Wright, H.E., Borodavko, P.S., van der Knaap, W.O., Ammann,
730 B., 2008. The role of pingos in the development of the Dzhangyskol lake-pingo
731 complex, central Altai Mountains, southern Siberia. Palaeogeography,
732 Palaeoclimatology, Palaeoecology, 257(4), 404-420.
733 Blyakharchuk, T.A., Chernova, N.A., 2013. Vegetation and climate in the Western
734 Sayan Mts according to pollen data from Lugovoe Mire as a background for
735 prehistoric cultural change in southern Middle Siberia. Quat. Sci. Rev. 75, 22-42.
736 Blyakharchuk, T.A., Kuryina, I.V., Pologova, N.N., 2019. Late Holocene dynamics of
737 vegetation cover and climate humidity in the southeastern sector of the West
738 Siberian Plain according to palynological and rhizopod studies of peat deposits.
739 Bulletin of Tomsk State University. Biology 45, 164–189. (in Russian)
740 Blyakharchuk, T.A., Pupysheva, M.A., 2022. Indication of fires in the thousand-year
741 history of Central Altai. Geography and Natural Resource, 4, 128-136 (In
742 Russian).
743 Blyakharchuk, T.A., van Hardenbroek, M., Pupysheva, M.A., Kirpotin, S.N.,
744 Blyakharchuk, P.A., 2024. Late Glacial and Holocene history of climate,
745 vegetation landscapes and fires in South Taiga of Western Siberia based on
746 radiocarbon dating and multi-proxy palaeoecological research of sediments from
747 Shchuchye Lake. Radiocarbon, 1-24, doi:10.1017/RDC.2024.103.
748 Blyakharchuk, T.A., 2020. Dynamics of vegetation cover and quantitative
749 palaeoclimatic reconstructions in the Western Sayan Mountains from the Late
750 Glacial period to the present time according to a palynological study of the
751 Yuzhno-Buybinskoe mire. In IOP Conference Series: Earth and Environmental
752 Science (Vol. 611, No. 1, p. 012026). IOP Publishing.
753 Blaauw, M., Christen, J.A., 2011. Flexible paleoclimate age-depth models using an
754 autoregressive gamma process. Bayesian Analysis 6, 457–474.
755 Carter, V. A., Bobek, P., Moravcová, A., Šolcová, A., Chiverrell, R. C., Clear, J. L.,
756 Kuneš, P., 2020. The role of climate-fuel feedbacks on Holocene biomass
757 burning in upper-montane Carpathian forests. Global and Planetary Change, 193,

758 103264.
759 Davis, M.B., 1965. A method for determination of absolute pollen frequency.
760 Handbook of paleontological techniques. San-Francisco-London: Freeman & Co,
761 P. 674–686.
762 Feurdean, A., Florescu, G., Tanţău, I., Vannière, B., Diaconu, A. C., Pfeiffer, M.,
763 Kirpotin, S., 2020. Recent fire regime in the southern boreal forests of western
764 Siberia is unprecedented in the last five millennia. Quat. Sci. Rev. 244, 106495.
765 Feurdean, A., Diaconu, A.C., Pfeiffer, M., Gałka, M., Hutchinson, S.M., Butiseaca, G.,
766 Gorina, N., Tonlkov, S., Niamir, A., Tantau, I., Zhang, H., Kirpotin S., 2022.
767 Holocene wildfire regimes in Western Siberia: Interaction between peatland
768 moisture conditions and the composition of plant functional types. Climate of the
769 Past 18, 1255–1274
770 Fu, B.J., Liu, G.H., Ouyang, Z.Y., 2013. Ecological regionalization in China. Beijing:
771 Science Press.
772 Furyaev, V.V., 1996. Role of Fire in Forest Development. Nauka Publications:
773 Novosibirsk (In Russia).
774 Ivanova, G.A., Kukavskaya, E.A., Ivanov, V.A., Conard, S.G., McRae, D.J., 2020.
775 Fuel characteristics, loads and consumption in Scots pine forests of central
776 Siberia. J. Forestry Res. 31(6), 2507-2524.
777 Jones, M.W., Smith, A., Betts, R., Canadell, J.G., Prentice, I.C., Le Quéré, C., 2020.
778 Climate change increases the risk of wildfires. ScienceBrief Rev. 116, 117.
779 Kasischke, E.S., 2000. Boreal ecosystems in the global carbon cycle. In: Kasischke,
780 E.S., Stocks, B.J. (Eds.), Fire, Climate Change, and Carbon Cycling in the Boreal
781 Forest. Ecological.
782 Kelly, R.F., Higuera, P.E., Barrett, C.M., Hu, F.S., 2011. A signal-to-noise index to
783 quantify the potential for peak detection in sediment–charcoal records. Quat. Res.
784 75, 11–17.
785 Khabarov, N., Krasovskii, A., Obersteiner, M., Swart, R., Dosio, A., San-Miguel-
786 Ayanz, J., Migliavacca, M., 2016. Forest fires and adaptation options in Europe.
787 Region. Environ. Chang. 16, 21-30.
788 Kharuk, V.I., Ponomarev, E.I., Ivanova, G.A., Dvinskaya, M.L., Coogan, S.C.,

Flannigan, M.D., 2021. Wildfires in the Siberian taiga. Ambio, 50(11), 1953-1974.

Krylov, A., McCarty, J.L., Potapov, P., Loboda, T., Tyukavina, A., Turubanova, S., Hansen, M.C., 2014. Remote sensing estimates of stand-replacement fires in Russia, 2002-2011. Environ. Res. Lett. 9(10), 105007.

Goldammer, J.G., Furyaev, V., 2013. Fire in ecosystems of boreal Eurasia (Vol. 48). Springer Science & Business Media.

Hastie, T.J., Tibshirani, R.J., 1986. Generalized additive models. Stat. Sci. 1 (3), 297–318.

Higuera, P.E., Brubaker, L.B., Anderson, P.M., Hu, F.S., Brown, T., 2009. Vegetation mediated the impacts of postglacial climate change on fire regimes in the southCentral Brooks Range, Alaska. Ecol. Monogr. 79, 201–219.

Higuera, P.E., Gavin, D.G., Bartlein, P.J., Hallett, D.J., 2010. Peak detection in sediment–charcoal records: impacts of alternative data analysis methods on fire-history interpretations. Int. J. Wildland Fire 19, 996–1114.

Hu, Y., Huang, X., Demberel, O., et al., 2024. Quantitative reconstruction of precipitation changes in the Mongolian Altai Mountains since 13.7 ka. Catena, 234, 107536.

Hu, Y., Huang, X., Li, Y., et al., 2025. Holocene fire dynamics in the Altai Mountains and its driving factors. Geophysical Research Letters, 52(9), e2025GL116309.

Huang, X., Peng, W., Rudaya, N., Grimm, E.C., Chen, X., Cao, X., Zhang, J., Pan, X., Liu, S., Chen, C., Chen, F., 2018. Holocene vegetation and climate dynamics in the Altai Mountains and surrounding areas. Geophys. Res. Lett. 45 (13), 6628-6636.

Lézine, A.M., Izumi, K., Achoundong, G., 2023. Mbi Crater (Cameroon) illustrates the relations between mountain and lowland forests over the past 15,000 years in western equatorial Africa. Quat. Int. 657, 67-76.

Li, Y., Zhang, Y., Wang, J., Wang, L., Li, Y., Chen, L., Zhao, L., Kong, Z., 2019. Preliminary study on pollen, charcoal records and environmental evolution of Alahake Saline Lake in Xinjiang since 4,700 cal yr BP. Quat. Int. 513, 8–17.

Li, Y., Zhang, D., Zhang, Y., Sun, A., Li, X., Huang, X., Zhang, Y., Li, Y., 2024.

Distentanging the late-Holocene human–environment interactions in the Altai Mountains within the Arid Central Asia. Palaeogeography, Palaeoclimatology, Palaeoecology, 654, 112466.

Liu, F., Liu, H., Xu, C., Shi, L., Zhu, X., Qi, Y., He, W., 2021. Old-growth forests show low canopy resilience to droughts at the southern edge of the taiga. Global Change Biology, 27(11), 2392-2402.

Lung, T., Lavalle, C., Hiederer, R., Dosio, A., Bouwer, L.M., 2013. A multi-hazard regional level impact assessment for Europe combining indicators of climatic and non-climatic change. Global and Environmental Change, 23, 522-536.

Marcott, S.A., Shakun, J.D., Clark, P.U., Mix, A.C., 2013. A reconstruction of regional and global temperature for the past 11,300 years. Science 339, 1198-1201.

Mo, L., Zohner, C. M., Reich, P. B., Liang, J., De Miguel, S., Nabuurs, G. J., Ortiz-Malavasi, E., 2023. Integrated global assessment of the natural forest carbon potential. Nature, 624(7990), 92-101.

Moritz, M.A., Batllori, E., Bradstock, R.A., Gill, A.M., Handmer, J., Hessburg, P.F., Leonard, J., McCaffrey, S., Odion, D.C., Schonennagel, T., Syphard, A.D., 2014. Learning to coexist with wildfire. Nature, 515(7525), 58-66.

Panyushkina, I.P., 2012. Climate-Induced changes in Population Dynamics of Siberian Scythians (700-250 B.C.). Climate, Landscapes and Civilizations. Geographycal Monograph Series 198, 145-154.

Pitkanen, A., Huttunen, P., Tolonen, K., Jungner, H., 2003. Long term fire frequency in the spruce-dominated forests of the Ulvinsalo strict nature reserve. Finland. Forest Ecology and Management, 176(1-3), 305-319.

Ponomarev, E.I., Kharuk, V.I., 2016. Wildfire occurrence in forests of the Altai-Sayan region under current climate changes. Contemporary Problems of Ecology, 9, 29-36.

Power, M.J., Marlon, J., Ortiz, N., et al., 2007. Changes in fire regimes since the Last Glacial Maximum: an assessment based on a global synthesis and analysis of charcoal data. Climate Dynamics, 30, 887-907.

Pupycheva, M.A., Blyakharchuk, T.A., 2024. Late Holocene dynamics of fires in the

forest-steppe zone (a case study of the Nikolaevsky Ryam) Geografiya I prirosnye resursy. 1, 54-61 (in Russian).

Reimer, P.J., Austin, W.E., Bard, E., Bayliss, A., Blackwell, P.G., Ramsey, C.B., Talamo, S., 2020. The IntCal20 Northern Hemisphere radiocarbon age calibration curve (0–55 cal kBP). Radiocarbon 62 (4), 725–757.

Rudaya, N., Sergey, K., Michał, S., Xianyong, C., Snezhana, Z., 2020. Postglacial history of the steppe Altai: climate, fire and plant diversity. Quat. Sci. Rev. 249, 106616.

Rudoy, A.N., Yatsuk, T.Yu., 1986. The palaeogeography of southeastern Altai. Chetvertichnaya geologiya i pervobytnaya arkheologiya. Thesis of conference, Ulan-Ude, 73–75.

Shi, C.M., Liang, Y., Gao, C., Wang, Q.H., Shu, L.F., 2020. Drought-modulated boreal forest fire occurrence and linkage with La Nina events in Altai Mountains Northwest China. Atmosphere, 11, 956.

Sun, A., Feng, Z.D., Ran, M., Zhang, C.J., 2013. Pollen-recorded bioclimatic variations of the last ~22,600 years retrieved from Achit Nuur core in the western Mongolian Plateau. Quat. Int. 311, 36-43.

Shi, C.M., Liang, Y., Gao, C., Wang, Q.H., Shu, L.F., 2020. Drought-modulated boreal forest fire occurrence and linkage with La Nina events in Altai Mountains Northwest China. Atmosphere, 11, 956.

Shumilova, L.V., 1962. Botanical Geography of Siberia. Tomsk University Press: Tomsk. (in Russian).

Slavnin, V.D., Sherstova L.I. 1999. Aerchaeologic-Ethnographic Essay of Northern Khakassia in the Area of Geological Polygon of Siberian High School). Tomsl Polytechnical University Press, Tomsk (in Russian)

Stockmarr, J.A., 1971. Tabletes with spores used in absolute pollen analysis. Pollen spores, 13, 61–621.

Tang, G., Yang, S., Miao, Y., et al., 2022. Grain size characteristics of microfossil charcoal and the environmental implications in loess deposits from Ganzi, Western Sichuan Plateau. Journal of Lanzhou University (Natural Sciences) 58 (03), 298–305 (in Chinese with English astract).

Stockmarr J.A., 1971. Tabletes with spores used in absolute pollen analysis. Pollen spores, 13, 61-621.

Umbanhowar Jr, C.E., Shinneman, A.L., Tserenkhand, G., Hammon, E.R., Lor, P., Nail, K., 2009. Regional fire history based on charcoal analysis of sediments from nine lakes in western Mongolia. Holocene 19(4), 611-624.

Unkelbach, J., Dulamsuren, C., Klinge, M., Behling, H., 2021. Holocene high-resolution forest-steppe and environmental dynamics in the Tarvagatai Mountains, northcentral Mongolia, over the last 9570 cal yr BP. Quat. Sci. Rev. 266, 107076.

Walker, X.J., Baltzer, J.L., Cumming, S.G., Day, N.J., Ebert, C., Goetz, S., Johnstone, J.F., Potter, S., Rogers, B.M., Schuur, E.A.G., Turetsky, M.R., Mack, M.C., 2019. Increasing wildfires threaten historic carbon sink of boreal forest soils. Nature, 572, 520-523.

Wang, W., Ma, Y.Z., Feng, Z.D., Narantsetseg, Ts, Liu, K.B., Zhai, X.W., 2011. A prolonged dry mid-Holocene climate revealed by pollen and diatom records from Lake Ugii Nuur in central Mongolia. Quat. Int. 229 (1e2), 74-83.

Wang, Z., Miao, Y., Zhao, Y., Zhang, Z., Zou, Y., Zhang, T., 2024. Preliminary exploration of the fire activity recorded by microcharcoal in surface sediments of Central and Western China. Quat. Sci. 44 (1), 201-213 (in Chinese with English astract).

Wood, S.N., 2017. Generalized Additive Models: An Introduction with R (2nd Edition). Chapman and Hall/CRC, pp1-476.

Xiao, Y., Xiang, L., Huang, X., et al., 2021. Moisture changes in the Northern Xinjiang Basin over the past 2400 years as Documented in Pollen Records of Jili Lake. Front. Earth Sci. 9, 741992.

Xiang, L., Huang, X., Sun, M., Panizzo, V. N., Huang, C., Zheng, M., Chen, F., 2023. Prehistoric population expansion in Central Asia promoted by the Altai Holocene climatic optimum. Nature Communications, 14(1), 3102.

Xinjiang Comprehensive Expedition Team, Institute of Botany, Chinese Academy of Sciences, 1978. Vegetation and its utilization in Xinjiang. Beijing: Science Press.

Zhang, D.L., Feng, Z.D., 2018. Holocene climate variations in the Altai Mountains

and the surrounding areas: a synthesis of pollen records. Earth Sci. Rev. 185, 847-869.

Zhang, D., Huang, X., Liu, Q., Chen, X., Feng, Z., 2022. Holocene fire records and their drivers in the westerlies-dominated Central Asia. Sci. Total Environ. 833, 155153.

Zhang, S.J., Lu, Y., Wei, W., Qiu, M., Dong, G., Liu, X., 2021. Human activities have altered fire-climate relations in arid Central Asia since ~1000 a BP: evidence from a 4200-year-old sedimentary archive. Sci. Bull. 66(8), 761-764.

Zhang, Y.Y., Feng, Z.D., 2024. Pollen-based quantitative reconstructions of Holocene climate at Gun Nuur in the northern Mongolian Plateau. Palaeogeography, Palaeoclimatology, Palaeoecology, 638, 112028.

Zhang, Y.Y., Zhang, D.L., 2025. Spatiotemporal patterns of pollen-based Holocene precipitation variations in the Altai Mountains and the surrounding areas. Global and Planetary Change, 251, 104832.

Zhao, Y., Liu, Y.L., Guo, Z.T., Fang, K.Y., Li, Q., Cao, X.Y., 2017. Abrupt vegetation shifts caused by gradual climate changes in central Asia during the Holocene. Sci. China Earth Sci. doi: 10.1007/s11430-017-9047-7

Zheng, B., Ciais, P., Chevallier, F., Yang, H., Canadell, J. G., Chen, Y., Zhang, Q., 2023. Record-high CO_2 emissions from boreal fires in 2021. Science, 379(6635), 912-917.

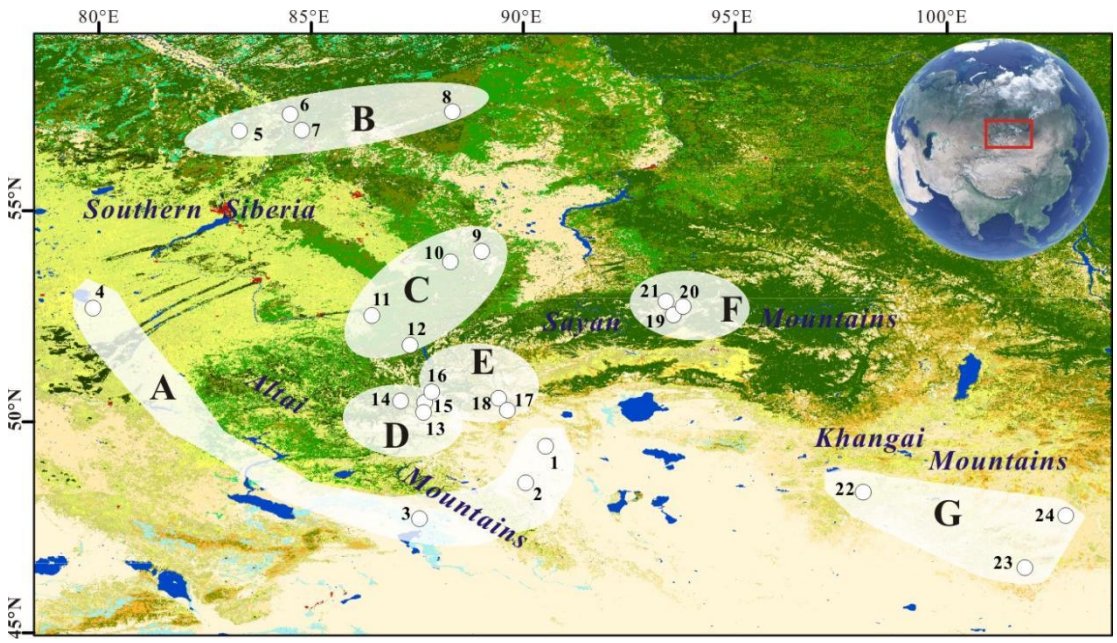

Fig. 1. Spatial distributions of the selected fossil pollen/charcoal sequences around the Altai-Sayan Mountains and adjacent plains. **Region A**: Achit Nuur (1), Tolbo Lake (2), Alahake Lake (3) and Kuchuk Lake (4); **Region B**: Rybnaya Mire (5), Plotnikovo Mire (6), Shchuchye Lake (7) and Ulukh–Chayakh Mire (8); **Region C**: Chudnoye Mire (9), Tundra Mire (10), Mokhovoe Bog (11) and Kuatang Mire (12); **Region D**: Dzhangyskol Lake (13), Uzunkol Lake (14) and Kendegelukol Lake (15); **Region E**: Tashkol Lake (16), Akkol Lake (17) and Grusha Lake (18); **Region F**: Buibinskoye Mire (19), Bezrybnoye Mire (20) and Lugovoe Peat (21); **Region G**: Olgi Lake (OL3) (22), Shireet Naiman Nuur (23) and Uggi Nuur (24).

.

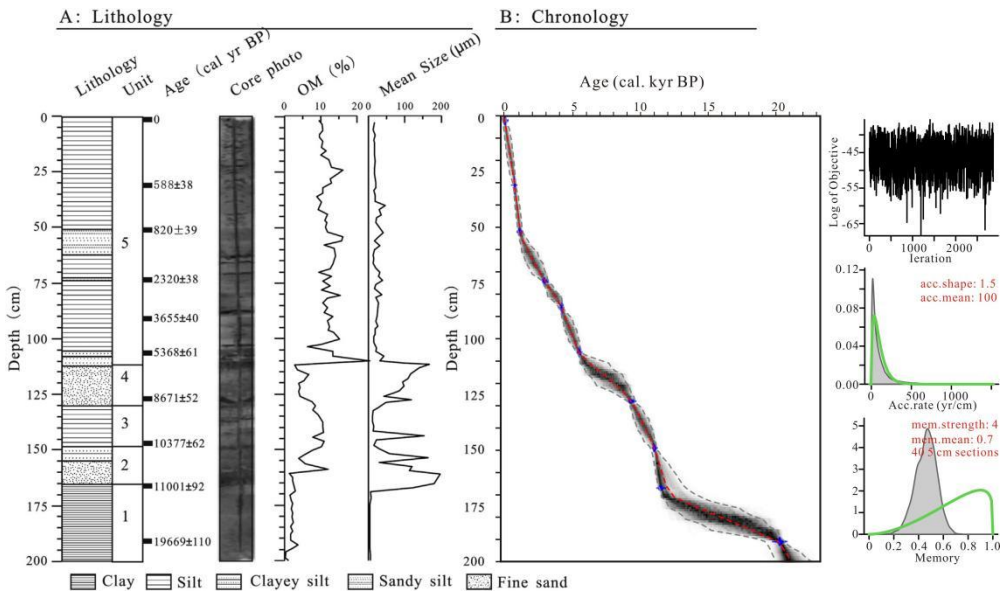

946

947 **Fig. 2.** Lithology, core photo, organic matter (OM), mean grain size and depth-age model in Achit

948 Nuur (modified from Sun et al., 2023).

949

950

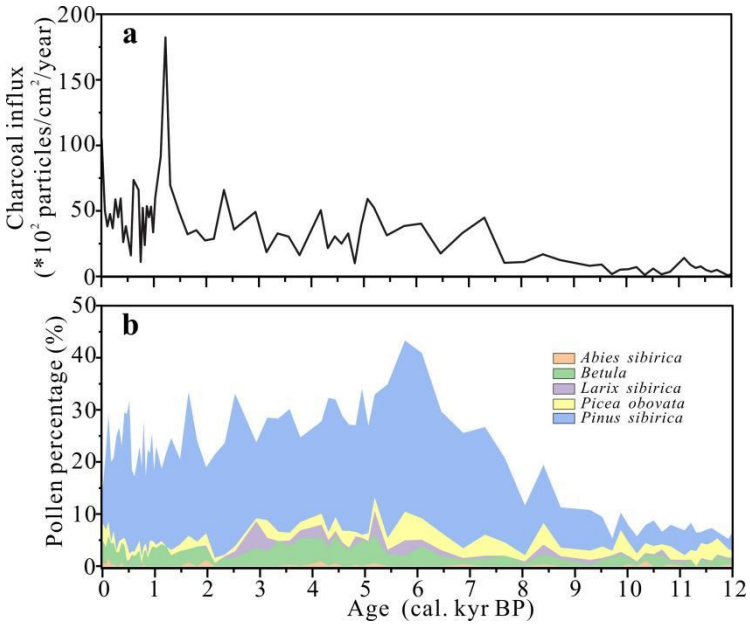

951

952 **Fig. 3.** Achit Nuur: charcoal influx (a) and vegetation change (b) (Sun et al., 2013; this study).

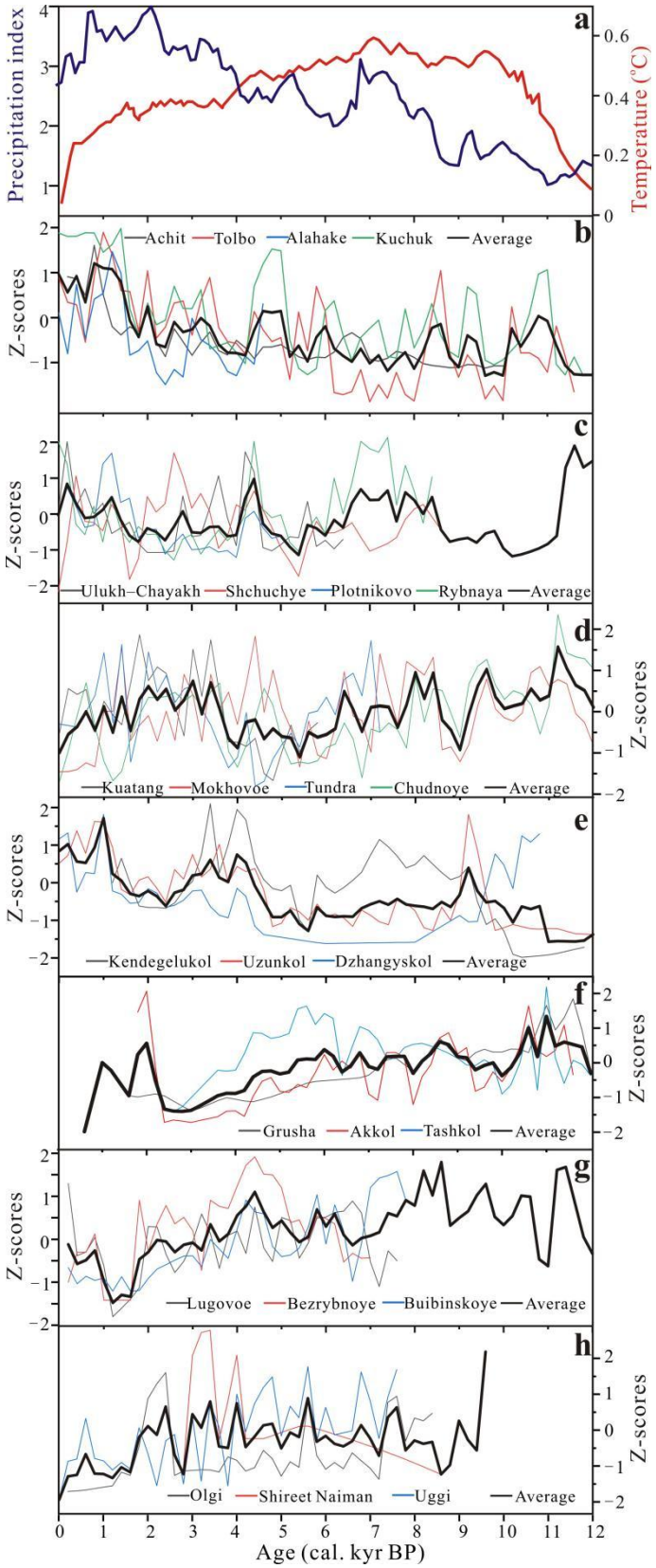

953

954 **Fig. 4.** Regional integrated charcoal influx (b-g) under the context of temperature (Marcott et al.,

955 2013) and precipitation index (a) in the Holocene interval (Zhang and Feng, 2018).

956

957 **Table 1** Detailed information of the selected sites around the Altai-Sayan Mountains and adjacent
958 plains.

Region	No.	Site Name	Lat. (N)	Long. (E)	Elev. (m a.s.l.)	Core length (cm)	Time interval (cal. kyr BP)	type of charcoal	References
A	1	Achit Nuur	49.42	90.52	1444	200	22.6	micro	this study
	2	Tolbo Lake	48.55	90.05	2080	253	10.3	micro+macro	Hu et al., 2025
	3	Alahake Lake	47.69	87.54	483	140	4.7	micro	Li et al., 2021
	4	Kuchuk Lake	52.69	79.84	98	255	13.1	macro	Rudaya et al., 2020
B	5	Rybnaya Mire	57.28	84.49	-	400	8.4	macro	Feurdean et al., 2022
	6	Plotnikovo Mire	56.88	83.30	120	225	5	macro	Feurdean et al., 2020
	7	Shchuchye Lake	57.13	84.61	80	331	12.8	micro	Blyakharchuk et al., 2024
	8	Ulukh–Chayakh Mire	57.34	88.32	-	348	8.5	macro	Feurdean et al., 2022
C	9	Chudnoye Mire	54.03	89.01	1147	590	12.7	micro	Blyakharchuk et al., 2024
	10	Tundra Mire	53.79	88.27	247	270	7.28	micro	Blyakharchuk et al., 2024
	11	Mokhovoe Bog	52.52	86.42	283	638	16.19	micro	Blyakharchuk, 2022
	12	Kuatang Mire	51.81	87.32	650	557	5.87	micro	Blyakharchuk et al., 2024
D	13	Dzhangyskol Lake	50.18	87.73	1800	380	13	micro	Blyakharchuk et al., 2008
	14	Uzunkol Lake	50.48	87.1	1985	285	12.02	micro	Blyakharchuk et al., 2004
	15	Kendegelukol Lake	50.50	87.63	2050	265	16.01	micro	Blyakharchuk et al.,

									2004
E	16	Tashkol Lake	50.45	87.67	2150	205	13.57	micro	Blyakharchuk et al., 2004
	17	Akkol Lake	50.25	89.62	2204	470	14	micro	Blyakharchuk et al., 2007
	18	Grusha Lake	50.38	89.42	2413	241	14.37	micro	Blyakharchuk et al., 2007
F	19	Buibinskoye Mire	52.84	93.52	1377	600	13.11	micro	Blyakharchuk et al., 2022
	20	Bezrybnoye Mire	52.81	93.50	1395	600	7.23	micro	Blyakharchuk et al., 2022
	21	Lugovoe Peat	52.85	93.35	1299	330	7.74	micro	Blyakharchuk et al., 2013
G	22	Olgi Lake(OL3)	48.32	98.01	2012	235	9.57	micro	Unkelbach et al., 2021
	23	Shireet Naiman Nuur	46.53	101.82	2429	178	7.4	micro	Barhoumi et al., 2024
	24	Uggi Nuur	47.77	102.78	1330	200	22.6	micro	Wang et al., 2011

Table 2 Correlation between the independent variables represented by pollen percentages (*Abies*, *Betula*, *Larix*, *Picea*, *Pinus sibirica*, *Pinus sylvestris* and their sum (i.e., forest cover) and the dependent variable (charcoal influx). The significance of each parameter is given by p values where ***p < 0.001; **p < 0.01; *p < 0.05.

Site Name	Independent variable	edf	ref.df	F value	p-value	Deviance explained
Achit Nuur	*Abies*	-	-	-	-	-
	Betula	2.75	3.47	3.40	0.02*	21%
	Larix	3.51	4.21	8.72	0.00***	41.9%
	Picea	1	1	11.36	0.001**	19.2%
	Pinus sibirica	2.73	3.41	5.70	0.001**	34.5%
	Pinus sylvestris	-	-	-	-	-
	Forest cover	2.92	3.69	8.02	0.00***	41.5%
Tolbo Lake	*Abies*	-	-	-	-	-
	Betula	6.96	8.01	1.76	0.09	7.04%
	Larix	1.03	1.07	0.03	0.95	0.03%
	Picea	2.97	3.75	4.47	0.002**	8.11%
	Pinus sibirica	2.68	3.39	9.55	0.00***	13.3%
	Pinus sylvestris	-	-	-	-	-
	Forest cover	2.98	3.75	8.96	0.00***	14.3%
Alahake Lake	*Abies*	1	1	0.57	0.45	1.1%
	Betula	1	1	4.19	0.04*	5.2%
	Larix	6.85	7.94	1.42	0.19	11.6%
	Picea	3.84	4.77	1.96	0.09	10%
	Pinus sibirica	5.59	6.77	1.85	0.09	13%
	Pinus sylvestris	-	-	-	-	-
	Forest cover	2.17	2.77	1.24	0.26	5.07%
Kuchuk Lake	*Abies*	1.21	1.40	3.80	0.03*	9.81%
	Betula	1.38	1.67	16.18	0.00***	25.2%
	Larix	1.11	1.21	0.01	0.98	0.19%
	Picea	1.16	1.30	1.31	0.30	2.29%
	Pinus sibirica	5.84	6.89	1.06	0.39	9.51%
	Pinus sylvestris	6.54	7.64	2.61	0.01*	25.5%
	Forest cover	3.59	4.47	1.22	0.28	11%
Rybnaya Mire	*Abies*	5.28	6.31	1.99	0.07	11.7%
	Betula	4.90	6.00	3.32	0.004**	18.4%
	Larix	7.07	8.11	1.95	0.07	20.6%
	Picea	8.15	8.79	14.1	0.00***	44.5%
	Pinus sibirica	6.74	7.86	1.68	0.12	16.6%
	Pinus sylvestris	2.03	2.54	1.06	0.35	4%
	Forest cover	7.00	8.10	3.06	0.003**	16.2%
Plotnikovo	*Abies*	3.12	3.88	0.70	0.55	16.7%

Mire	*Betula*	2.69	3.36	1.40	0.26	19.6%
	Larix	1	1	4.09	0.06	20.1%
	Picea	2.12	2.65	1.54	0.26	15.1%
	Pinus sibirica	1.68	2.11	0.41	0.7	4.85%
	Pinus sylvestris	2.01	2.53	1.50	0.23	14.7%
	Forest cover	4.43	5.21	4.07	0.004**	39.7%
Schuchye Lake	*Abies*	4.78	5.85	5.39	0.00***	37.4%
	Betula	1	1	5.29	0.03*	10.8%
	Larix	1	1	63.71	0.00***	45.4%
	Picea	2.19	2.71	3.77	0.02*	17.5%
	Pinus sibirica	1	1	27.6	0.00***	30.8%
	Pinus sylvestris	3.15	3.90	3.31	0.02*	21.2%
	Forest cover	2.10	2.52	7.91	0.00***	24.7%
Ulukh–Chay akh Mire	*Abies*	6.38	7.52	1.60	0.18	29.4%
	Betula	1	1	6.44	0.01*	13.4%
	Larix	2.54	3.16	2.46	0.07	17.5%
	Picea	2.45	3.12	1.46	0.23	16.7%
	Pinus sibirica	1	1	0.66	0.42	1.82%
	Pinus sylvestris	1	1	4.43	0.04*	10.3%
	Forest cover	4.26	5.08	1.46	0.22	16.9%
Chudnoye Lake	*Abies*	1.75	2.17	2.09	0.14	8.52%
	Betula	1.23	1.42	10.54	0.001**	23.5%
	Larix	2.06	2.57	3.84	0.03*	14.7%
	Picea	1.99	2.44	11.76	0.00***	30.3%
	Pinus sibirica	4.33	5.25	3.38	0.01*	26.6%
	Pinus sylvestris	1	1	6.59	0.01*	11.6%
	Forest cover	1	1	1.97	0.17	3.5%
Tundra Mire	*Abies*	2.16	2.75	0.78	0.57	3.83%
	Betula	1	1	3.27	0.07	4.44%
	Larix	6.41	7.35	4.32	0.00***	22.7%
	Picea	1	1	0.09	0.77	0.13%
	Pinus sibirica	2.39	2.99	0.83	0.46	4.66%
	Pinus sylvestris	3.03	3.78	0.79	0.49	5.83%
	Forest cover	1	1	2.79	0.10	3.53%
Mokhove Bog	*Abies*	1.83	2.31	1.12	0.38	3.65%
	Betula	6.81	7.88	2.07	0.05	17.2%
	Larix	1.09	1.17	0.24	0.63	0.59%
	Picea	2.59	3.22	3.54	0.02*	11.9%
	Pinus sibirica	1	1	0.00	0.96	0.003%
	Pinus sylvestris	4.46	5.49	1.78	0.11	13%
	Forest cover	5.04	6.19	0.91	0.48	10.3%
Kuatang Mire	*Abies*	2.45	3.14	2.78	0.04*	13.8%
	Betula	1	1	29.13	0.00***	24.5%

	Larix	1	1.00	0.06	0.81	0.08%
	Picea	6.72	7.79	1.19	0.31	13.4%
	Pinus sibirica	1.43	1.74	2.92	0.05*	6.90%
	Pinus sylvestris	1	1	5.83	0.02*	6.51%
	Forest cover	1	1	9.24	0.003**	10.9%
Dzhangyskol Lake	*Abies*	3.64	4.53	0.45	0.79	16.9%
	Betula	1.79	2.23	0.37	0.77	7.12%
	Larix	1	1	0.05	0.83	0.33%
	Picea	3.92	4.80	0.82	0.51	24.8%
	Pinus sibirica	1.70	2.12	0.35	0.73	7.06%
	Pinus sylvestris	3.05	3.75	1.22	0.29	22.8%
	Forest cover	2.39	3.04	0.67	0.58	15.6%
Uzunkol Lake	*Abies*	1	1	5.329	0.02*	7.04%
	Betula	4.92	5.99	3.22	0.01**	29.4%
	Larix	1	1	14.38	0.00***	22.1%
	Picea	5.99	7.12	5.03	0.00***	40.1%
	Pinus sibirica	2.04	2.57	1.99	0.14	14.7%
	Pinus sylvestris	4.79	5.81	2.85	0.02*	29.3%
	Forest cover	2.17	2.69	1.39	0.27	14.2%
Kendegelukol Lake	*Abies*	4.93	5.97	2.63	0.04*	41.4%
	Betula	5.87	7.04	2.78	0.02*	49.4%
	Larix	1	1	3.11	0.09	9.63%
	Picea	2.99	3.73	2.19	0.08	29.4%
	Pinus sibirica	2.25	2.78	2.26	0.09	28.9%
	Pinus sylvestris	1	1	18.48	0.00***	40%
	Forest cover	1.57	1.91	3.58	0.06	26.9%
Tashkol Lake	*Abies*	1	1	0.02	0.90	0.09%
	Betula	1	1	0.08	0.79	0.36%
	Larix	1.56	1.92	0.20	0.82	3.52%
	Picea	6.69	7.81	2.35	0.04*	40.7%
	Pinus sibirica	1	1	0.004	0.95	0.02%
	Pinus sylvestris	1	1	0.02	0.89	0.09%
	Forest cover	3.00	3.75	0.90	0.48	17%
Akkol Lake	*Abies*	1.76	2.11	0.79	0.43	4.83%
	Betula	1	1	0.96	0.33	1.76%
	Larix	6.53	7.59	1.94	0.08	30.4%
	Picea	2.41	3.03	6.77	0.00***	31.6%
	Pinus sibirica	4.35	5.41	1.90	0.1	23%
	Pinus sylvestris	1	1	10.12	0.002**	18.9%
	Forest cover	8.47	8.92	5.49	0.00***	55.1%
Grusha Lake	*Abies*	1	1	0.62	0.44	2.75%
	Betula	1	1	0.88	0.36	3.93%

	Larix	3.81	4.58	3.44	0.02*	49.3%
	Picea	2.18	2.71	3.30	0.05*	35.80%
	Pinus sibirica	1	1	0.60	0.45	2.67%
	Pinus sylvestris	1.39	1.66	0.19	0.76	4.67%
	Forest cover	2.55	3.18	12.7	0.00***	71.1%
	Abies	1.15	1.29	0.31	0.75	1.16%
	Betula	1.74	2.20	1.63	0.22	8.85%
Bezrybnoe	*Larix*	2.58	3.14	0.32	0.79	4.76%
Mire	*Picea*	1	1	2.13	0.15	4.49%
	Pinus sibirica	1.37	1.66	0.39	0.75	2.18%
	Pinus sylvestris	6.47	7.53	1.69	0.13	28.1%
	Forest cover	1	1	0.01	0.93	0.02%
	Abies	2.71	3.39	4.85	0.004**	29.6%
	Betula	2.11	2.69	2.29	0.10	17.4%
Buibinskoye	*Larix*	1	1	1.16	0.29	2.83%
Mire	*Picea*	1.52	1.87	0.71	0.40	4.85%
	Pinus sibirica	2.02	2.57	2.70	0.05	17.4%
	Pinus sylvestris	1	1	3.78	0.06	7.42%
	Forest cover	3.61	4.42	2.47	0.06	22.6%
	Abies	1	1	6.32	0.02*	15.3%
	Betula	1	1	0.23	0.64	0.79%
Lugovoe	*Larix*	5.00	5.91	3.89	0.01**	43.5%
Mire	*Picea*	4.00	4.95	2.41	0.07	35.8%
	Pinus sibirica	3.43	4.28	2.20	0.09	31%
	Pinus sylvestris	8.81	8.98	3.21	0.01*	60.5%
	Forest cover	1.14	1.27	0.20	0.67	2.29%
	Abies	-	-	-	-	-
	Betula	4.89	5.96	2.91	0.02*	34.5%
	Larix	4.32	5.29	2.68	0.03*	35.6%
Olgi Lake	*Picea*	3.8	4.65	4.20	0.003**	35.7%
	Pinus sibirica	8.62	8.89	45.23	0.00***	27.9%
	Pinus sylvestris	-	-	-	-	-
	Forest cover	1.74	2.21	7.46	0.00***	33.3%
	Abies	-	-	-	-	-
	Betula	2.57	3.211	3.82	0.01*	20.7%
Shireet	*Larix*	1	1	1.59	0.21	2.83%
Naiman Nuur	*Picea*	1	1	6.55	0.01*	9.70%
	Pinus sibirica	3.98	4.91	4.02	0.003**	27.5%
	Pinus sylvestris	1	1	7.99	0.01**	12%
	Forest cover	4.01	4.96	6.38	0.00***	37.4%
	Abies	-	-	-	-	-
Uggi Nuur	*Betula*	6.49	7.59	2.02	0.06	8.65%
	Larix	6.48	0.06	104.4	0.00***	12.2%

	Picea	1	1	0.18	0.67	0.1%
	Pinus sibirica	8.55	8.94	6.19	0.00***	19.4%
	Pinus sylvestris	-	-	-	-	-
	Forest cover	8.07	8.76	5.72	0.00***	18.4%

966

967